HHS Public Access

Author manuscript

Nano Lett. Author manuscript; available in PMC 2015 July 19.

Published in final edited form as:

Nano Lett. 2013 July 10; 13(7): 3256–3261. doi:10.1021/nl4013776.

Tailorable Plasmonic Circular Dichroism Properties of Helical Nanoparticle Superstructures

Chengyi Song[†], **Martin G. Blaber**[‡], **Gongpu Zhao**[§], **Peijun Zhang**[§], **H. Christopher Fry**[‖], **George C. Schatz**[‡], and **Nathaniel L. Rosi**[†]

Nathaniel L. Rosi: nrosi@pitt.edu

[†]Department of Chemistry, University of Pittsburgh, 219 Parkman Avenue, Pittsburgh, Pennsylvania 15260, United States

[‡]Department of Chemistry, Northwestern University, 2145 Sheridan Road, Evanston, Illinois 60208, United States

[§]Department of Structural Biology, University of Pittsburgh, School of Medicine, 3501 Fifth Avenue, Pittsburgh, Pennsylvania 15260, United States

[‖]Center for Nanoscale Materials, Argonne National Laboratory, 9700 South Cass Avenue, Argonne, Illinois 60439, United States

Abstract

We utilize a peptide-based methodology to prepare a diverse collection of double-helical gold nanoparticle superstructures having controllable handedness and structural metrics. These materials exhibit well-defined circular dichroism signatures at visible wavelengths owing to the collective dipole–dipole interactions between the nanoparticles. We couple theory and experiment to show how tuning the metrics and structure of the helices results in predictable and tailorable chirooptical properties. Finally, we experimentally and theoretically demonstrate that the intensity, position, and nature of the chirooptical activity can be carefully adjusted via silver overgrowth. These studies illustrate the utility of peptide-based nanoparticle assembly platforms for designing and preparing complex plasmonic materials with tailorable optical properties.

Keywords

Chiral nanostructures; circular dichroism; nanoparticle assembly; chirality; surface plasmon

Chiral plasmonic nanoparticle superstructures are attractive synthetic targets because of their potential applications as circular polarizers, chirooptical sensors, and negative refraction materials.(1–5) One of the most effective ways to finely adjust the chirooptical properties of chiral plasmonic nanoparticle superstructures is to precisely control their metrics and structural parameters. Many approaches have been utilized to prepare chiral nanoparticle assemblies.(6–23) Of these, biomolecule-based approaches are the most common, because biomolecules, such as peptides and nucleic acids, can both be programmed to assemble into

Correspondence to: Nathaniel L. Rosi, nrosi@pitt.edu.

chiral architectures and also designed to bind or associate to specific nanoparticle surfaces.(6–17) Helical structures represent a unique subcategory of chiral nanoparticle assemblies.(12, 13, 15–17, 20, 22–24) Following early reports detailing peptide-directed assembly of helical gold nanoparticle superstructures(12) and nucleic-acid-directed assembly of helical nanoparticle architectures,(13) several groups employed peptides or nucleic acids to prepare helical nanoparticle superstructures that exhibit targeted chirooptical properties.(15–17) In order to control and tailor the chirooptical properties of helical nanoparticle assemblies, an assembly methodology should allow one to precisely and simultaneously control the position, organization, and size of the nanoparticles within the nanoparticle superstructure product.

We recently reported a conceptual framework and synthetic methodology for designing and preparing nanoparticle superstructures that utilizes carefully designed peptide conjugate molecules for precisely directing the synthesis and assembly of nanoparticles.(12) We demonstrated that these strategies and methods are very useful for targeting, preparing, and tailoring the metrics and structural parameters of a diverse family of 1D gold nanoparticle superstructures, including chiral double helices(12, 25) and linear chains,(26) as well as a collection of discrete hollow spheres consisting of either gold(27, 28) or cobalt–platinum nanoparticles.(29) The precision of nanoparticle placement and the structural integrity of the resulting nanoparticle superstructures are key distinguishing features of this methodology. In this report, we utilize a peptide-based toolkit to prepare a unique and diverse collection of chiral gold nanoparticle double-helical superstructures comprising both left- and right-handed structures with tailorable nanoparticle sizes (Figure 1) and compositions. We demonstrate for the first time that these materials exhibit chiral plasmonic optical behavior that can be carefully tuned by adjusting their structure and composition.

C_{12}-l-PEP_{Au} conjugates (C_{12}-PEP_{Au} = [$C_{11}H_{23}CO$]-AYSSGAPPMPPF), comprising l-amino acids, were used to construct left-handed gold nanoparticle double helices using established methods.(12, 25) In previous work, we demonstrated that C_{12}-l-PEP_{Au} conjugates, under certain conditions, assemble into left-handed twisted nanofibers having a regular pitch of ~84 nm.(12) We reasoned that the left-handed helicity of these fibers resulted from the chirality of the l-amino acid within the C_{12}-l-PEP_{Au} conjugates. Therefore, C_{12}-d-PEP_{Au} should assemble into compositionally identical fibers as C_{12}-l-PEP_{Au}, but with a right-handed twisted ribbon structure. We thus prepared C_{12}-d-PEP_{Au} conjugates and used these to construct right-handed gold nanoparticle double helices. Transmission electron microscopy (TEM) studies confirmed that both left- and right-handed double helices (i) consist of spherical gold nanoparticles (left-handed helices particle diameter = 5.74 ± 0.75 nm; right-handed helices particle diameter = 5.25 ± 0.79 nm), (ii) exhibit a regular pitch (~82 nm), interhelical distance (~7.5 nm), and interparticle distance (~1.7 nm), and (iii) extend lengthwise well into the micrometer regime (Figure 2a,b,d,e, Supporting Information Figures S4 and S5). Three-dimensional electron tomography reconstructions of nanoparticle double helices definitively reveal the handedness of these structures: C_{12}-l-PEP_{Au} derived double helices are indeed left-handed (Figure 2c) and C_{12}-d-PEP_{Au} derived double helices are right-handed (Figure 2f). To our knowledge, this is the first reported example of using a peptide-based nanoparticle assembly strategy to control the handedness of helical nanoparticle superstructures.

The gold nanoparticle double helices were incubated for one day in the gold salt precursor solution until the gold nanoparticles grew to ~8 nm in diameter (interhelical distance ~6.5 nm; interparticle distance ~1.4 nm; pitch ~82 nm; see Figure 1, Supporting Information Figures S6–S9). Circular dichroism (CD) spectroscopy was employed to examine the optical activity of the assembled structures in solution. In the ultraviolet region, the left-handed and the right-handed double helices have a negative and positive CD, respectively, at ~220 nm (Supporting Information Figure S10), which results from the chirality of the self-assembled peptide conjugates underlying the gold nanoparticle assemblies. We expected that the double-helical structures would exhibit visible chirooptical activity at wavelengths corresponding to the collective surface plasmon resonance of the assembled gold nanoparticles. Indeed, the left- and right-handed helices respectively, produce vertically mirrored negative and positive CD signals at 562 nm (Figure 3a), consistent with the existence of the collective surface plasmon resonance (Supporting Information Figure S11). Others have observed visible plasmonic circular dichroism for peptide-capped gold nanoparticles;(30) however, we do not observe a CD signal in the visible range for nonassembled PEP_{Au}-capped gold nanoparticles,(31) (Supporting Information Figure S12) which suggests that the observed circular dichroism effect results from the spatial arrangement of the gold nanoparticles within the superstructures. Having measured the visible chirooptical activity of these nanoparticle superstructures, we next used computational methods to first model the experimental results and then predict how changing the structural metrics of the assemblies might affect the chirooptical response. This work is similar to recent studies,(4, 32) but we utilize a different approach.

Small metal nanoparticles interact primarily through dipole–dipole interactions, but higher order multipoles contribute to the position and strength of the ensemble localized surface plasmon resonance (LSPR) as the interparticle distance is reduced. For this reason, we chose to model the chiral ensemble of metallic nanoparticles within the framework of the discrete dipole approximation (DDA).(33, 34) In this method, individual particles are described by thousands of dipoles, such that higher order multipole effects are accounted for. The CD response is determined by averaging the difference in extinction cross sections, *Q*, between left ($|\mathrm{L}\rangle$) and right ($|\mathrm{R}\rangle$) circularly polarized plane waves for many orientations of the helical superstructure

$$\mathrm{CD}=\langle Q_{|\mathrm{L}\rangle}-Q_{|\mathrm{R}\rangle}\rangle_{\Omega} \quad (1)$$

where Ω indicates the set of orientations of the helix with respect to the incident wave-vector (see the Supporting Information for details on the choice of orientations(35–38)). A number of experimental and theoretical studies have been presented on one-dimensional chains of spherical gold(39–42) and silver(41) nanoparticles, and simulations show that in general the LSPR shift associated with increasing the length of a 1D chain of particles saturates at around 10 particles.(43, 44) For this reason, we have chosen to simulate a short helix, consisting of only a single helical period of around 80 nm in length, or a minimum of 12 spheres per helix. The computational model accurately reproduces the experimental CD spectrum of the gold nanoparticle double helices (Figure 3b), particularly for the ~560 nm CD signature, which arises when the incident field propagates parallel to the helical axis. The red-shifted ~600 nm feature appears when the field propagates perpendicular to the

helical axis. In the experiment, this feature appears further to the red (Figure 3a), primarily due to variations in interparticle distance. Figure S14 in the Supporting Information shows that averaging the CD spectra from helices with interparticle distances ranging from 1.0 to 2.0 nm leaves the 560 nm feature unchanged but causes the ~600 nm peak to red shift.

In 1D chains of particles, the longitudinal plasmon resonance (λ_p, polarization parallel to the long axis of the chain) is related to the plasmon resonance of an individual sphere in the chain (λ_s) and the ratio of the particle diameter (D) to the interparticle gap (G) via the empirical relation(44)

$$\lambda_p = \lambda_s A\left(\frac{D}{G}\right)^B + \lambda_s \quad (2)$$

where A is a proportionality constant (typically around 0.01 nm^{-1}) and B is an exponent that depends on the length of the chain; for sufficiently long chains, it approaches 1 from below. For this reason, we posit that the interparticle spacing along the axis of the helix will play a larger role in determining the optical response of the assembly than the interhelical distance. Indeed, simulations show that when the interhelical distance is increased from the experimental mean of approximately 7.0 nm, only small variations in the position and intensity of the CD spectrum are evident (Supporting Information Figure S13). If the interhelical distance is reduced to 4.0 nm, the transverse resonance increases in magnitude by approximately 2%, and a slight blue shift of the high energy peak is apparent.

Modifications to the interparticle gap (closest nearest neighbor distance) from 1.5 nm (close to the experimental value of 1.4 nm) can shift the high energy peak in the CD spectrum from 560 nm (Figure 3b) to approximately 540 nm for an interparticle distance of 2.0 nm (Supporting Information Figure S14). If the interparticle gap is reduced to 1.0 nm, the peak in the CD spectrum red shifts to ~580 nm (Supporting Information Figure S14). As gold is more polarizable in the near-infrared than in the visible,(45) shifting the LSPR to the red increases the extinction cross section of the assemblies and hence increases the magnitude of the CD response.

Our model predicts that increasing the radius of the nanoparticles will have the same effect as decreasing the interparticle distance (namely a red shift of the longitudinal LSPR and increase in the extinction cross section). As such, we added additional aliquots of $HAuCl_4/H_2O$ to samples of left- and right-handed gold helices (particle diameters: left-handed helices = 8.64 ± 1.43 nm; right-handed helices = 7.59 ± 1.22 nm) (Supporting Information Figures S15 and S16) suspended in HEPES buffer to yield product helices with larger nanoparticles (particle diameters: left-handed helices = 10.55 ± 0.75 nm; right-handed helices = 10.70 ± 2.07 nm) (Supporting Information Figures S17 and S18). CD measurements of these samples showed that signal intensity dramatically increased and the CD peak red-shifted (Supporting Information Figure S19). The CD signal for left-handed helices shifted from 571 to 594 nm while the CD signal for right-handed helices shifted from 566 to 602 nm (Supporting Information Figure S19). These results were consistent with our simulations that showed that when the particle diameter of left-handed gold helices is increased from the mean experimental value of approximately 8.0–11.0 nm, the ~560 nm

dip shifts to above ~575 nm, and the magnitude of the peak approximately doubles (Supporting Information Figure S20). In summary, carefully controlling structural parameters allows one to tune the macrooptical activity of these nanohelical assemblies. Our theoretical model based on classical electrodynamics provides a means of interpreting and predicting the chirooptical behavior.

On the basis of our theoretical prediction, double helices consisting of small gold nanoparticles should result in a CD signal shift to shorter wavelengths along with a concomitant decrease in signal intensity. Our experimental data bears this out to some extent. As we decrease the nanoparticle size, we observe a decrease in the CD signal along with a slight blue shift, although the CD signal is quite weak (Supporting Information Figures S21 and S22). In order to generate a strong blue-shifted CD response, we coated the gold nanoparticle double helices with silver. Specifically, we deposited varying amounts of silver onto freshly prepared gold nanoparticle double helices (~8 nm particle diameters) to control the thickness of the silver shell. Scanning TEM (STEM) image and energy dispersive spectroscopy (EDS) data indicate that the silver-coated double helices consist of gold nanoparticles (white core) coated with silver (gray shell) (Supporting Information Figure S23). CD spectra and TEM images (Figure 4a,c and Supporting Information Figures S24–S29, respectively) reveal that double helices with larger particles exhibit stronger CD signal at shorter wavelength. When the double helices are coated with a very thin silver shell (~0.5 nm), the CD intensity increases and exhibits the same sign as the original gold nanoparticle helices. However, if the gold nanoparticle double helices are coated with a thick silver shell, the CD intensity appears to significantly increase yet with the opposite sign of the original gold helices. Again, to confirm that the observed CD response results from the assembled superstructure, we collected CD data for nonassembled peptide-coated gold particles coated with silver; these particles did not exhibit a CD signal in the visible (Supporting Information Figures S30 and S31). We employed theory and simulation to understand the CD data from the silver-coating experiments. We present the simulated extinction spectra for a double helix consisting of just gold spheres and of gold spheres coated with 1.0, 1.5, and 2.0 nm of silver (Supporting Information Figure S32). The introduction of silver onto the gold spheres causes the appearance of a band at around 375 nm that is associated with the silver. Additionally, the longitudinal resonance shifts to the blue as the silver thickness increases, which is a direct effect of the difference in the wavelength position of the interband transitions between the two metals: those in silver are in the UV, and those of gold are in the blue region of the spectrum. As more silver is added, the polarizability (and hence the extinction) of the nanoparticles increases as silver is more polarizable than gold in this region of the spectrum.(45) These effects conspire to blue shift the CD spectrum (Figure 4b,d) and the 550 nm dip in Figure 4a,c appears to change sign when the silver-coating thickness increases from approximately 0.5 nm to above approximately 1.0 nm. The simulations (Figure 4b,d) indicate that this effect can be explained by a large blue shift in the resonances of the double-helices when silver is introduced into the system together with the increase in intensity.

The experimental CD spectra (Figure 4a,c) exhibit only small CD response in the blue in comparison to the features at approximately 550 nm, whereas the simulated spectra exhibit peaks and troughs of approximately equal magnitude. This can be explained by variations in

the interparticle gap along the helix. Supporting Information Figure S33 shows the effect of varying the interparticle gap between 0.5 and 1.5 nm: reducing the gap causes the CD response to red shift. Regions of the spectra that show negative CD signal at gaps of 1.5 nm (for example: purple trace, Figure 4d) are reduced in magnitude because the negative signal in this region is offset by positive CD response of locations on the helix where the particles are 0.5 nm apart. This amounts to an interference-like effect between helices with larger (~1.5 nm) and smaller (~0.5 nm) interparticle gaps.

If the particles are touching (or conjoined) for long regions of the helix then the CD response is flat across the visible due to a lack of dipole–dipole coupling between particles (i.e., the system resembles a twisted nanowire with a plasmonic response that has shifted to the IR, see Supporting Information Figure S33).

The peptide-based assembly toolkit allows for the construction of a diverse set of gold nanoparticle double helices with tunable structures, handedness, and physical properties. We used this toolkit to prepare left- and right-handed gold nanoparticle double helices that exhibit well-defined plasmonic circular dichroism signals. By coupling predictions from theory and simulation with experiment, we demonstrated that tuning the nanoparticle size can affect the chirooptical properties and that altering the composition of the helices can dramatically affect the position and intensity of the plasmonic CD signal. In future experiments, we aim to orient and assemble the helices to obtain a much higher chirooptical response. Also, we aim to design peptide conjugates for preparing helices with different pitch, interparticle distance, and interhelical distance to further experimentally assess how these parameters affect the CD response. The work reported herein indicates that this peptide-based nanoparticle assembly methodology is a powerful means of preparing tailorable plasmonic nanostructures with carefully tunable chirooptical properties.

Supplementary Material

Refer to Web version on PubMed Central for supplementary material.

Acknowledgment

The authors are grateful for financial support from the National Science Foundation (DMR-0954380, NLR), the Air Force Office of Scientific Research (FA9550-11-1-0275, N.L.R., and G.C.S.) and the National Institutes of Health (GM085043, P.Z.). This work was performed in part at the Center for Nanoscale Materials, a U.S. Department of Energy, Office of Science, Office of Basic Energy Sciences User Facility under Contract No. DE-AC02-06CH11357. The authors thank the Peterson NFCF and the MEMS Department for provision of access to TEM. The authors thank Professor W. Seth Horne for helpful discussions regarding the acquisition of CD data and Dr. Susheng Tan for assisting with STEM and EDS measurements.

References

1. Gansel JK, Thiel M, Rill MS, Decker M, Bade K, Saile V, von Freymann G, Linden S, Wegener M. Science. 2009; 325:1513. [PubMed: 19696310]
2. Pendry JB. Science. 2004; 06:1353. [PubMed: 15550665]
3. Zhu Y, Xu L, Ma W, Xu Z, Kuang H, Wang L, Xu C. Chem. Commun. 2012; 48:11889.
4. Fan Z, Govorov AO. Nano Lett. 2010; 10:2580. [PubMed: 20536209]
5. Govorov AO, Gun'ko YK, Slocik JM, Gerard VA, Fan Z, Naik RRJ. Mater. Chem. 2011; 21:16806.
6. Tan SJ, Campolongo MJ, Luo D, Cheng W. Nat. Nanotechnol. 2011; 6:268. [PubMed: 21499251]

7. Shemer G, Krichevski O, Markovich G, Molotsky T, Lubitz I, Kotlyar AB. J. Am. Chem. Soc. 2006; 128:11006. [PubMed: 16925401]
8. George J, Thomas KG. J. Am. Chem. Soc. 2010; 132:2502. [PubMed: 20136136]
9. Yan W, Xu L, Xu C, Ma W, Kuang H, Wang L, Kotov NA. J. Am. Chem. Soc. 2012; 134:15114. [PubMed: 22900978]
10. Fu X, Wang Y, Huang L, Sha Y, Gui L, Lai L, Tang Y. Adv. Mater. 2003; 15:902.
11. Mastroianni AJ, Claridge SA, Alivisatos AP. J. Am. Chem. Soc. 2009; 131:8455. [PubMed: 19331419]
12. Chen C-L, Zhang P, Rosi NL. J. Am. Chem. Soc. 2008; 130:13555. [PubMed: 18800838]
13. Sharma J, Chhabra R, Cheng A, Brownell J, Liu Y, Yan H. Science. 2009; 323:112. [PubMed: 19119229]
14. Chen W, Bian A, Agarwal A, Liu L, Shen H, Wang L, Xu C, Kotov NA. Nano Lett. 2009; 9:2153. [PubMed: 19320495]
15. Guha S, Drew MGB, Banerjee A. Small. 2008; 4:1993. [PubMed: 18949791]
16. Kuzyk A, Schreiber R, Fan Z, Pardatscher G, Roller E-M, Hogele A, Simmel FC, Govorov AO, Liedl T. Nature. 2012; 483:311. [PubMed: 22422265]
17. Shen X, Song C, Wang J, Shi D, Wang Z, Liu N, Ding B. J. Am. Chem. Soc. 2011; 134:146. [PubMed: 22148355]
18. Gerard VA, Gun'ko YK, Defrancq E, Govorov AO. Chem. Commun. 2011; 47:7383.
19. Guerrero-Martínez A, Auguié B, Alonso-Gómez JL, Džolić Z, Gómez-Graña S, Žinić M, Cid MM, Liz-Marzán LM. Angew. Chem., Int. Ed. 2011; 50:5499.
20. Wang R-Y, Wang H, Wu X, Ji Y, Wang P, Qu Y, Chung T-S. Soft Matter. 2011; 7:8370.
21. Qi H, Shopsowitz KE, Hamad WY, MacLachlan MJ. J. Am. Chem. Soc. 2011; 133:3728. [PubMed: 21355559]
22. Wang Y, Wang Q, Sun H, Zhang W, Chen G, Wang Y, Shen X, Han Y, Lu X, Chen H. J. Am. Chem. Soc. 2011; 133:20060. [PubMed: 22091894]
23. Sone ED, Zubarev ER, Stupp SI. Angew. Chem. Int. Ed. 2002; 41:1705.
24. Yang M, Kotov NA. J. Mater. Chem. 2011; 21:6775.
25. Chen C-L, Rosi NL. J. Am. Chem. Soc. 2010; 132:6902. [PubMed: 20429558]
26. Hwang L, Chen C-L, Rosi NL. Chem. Commun. 2011; 47:185.
27. Song C, Zhao G, Zhang P, Rosi NL. J. Am. Chem. Soc. 2010; 132:14033. [PubMed: 20853836]
28. Hwang L, Zhao G, Zhang P, Rosi NL. Small. 2011; 7:1939.
29. Song C, Wang Y, Rosi NL. Angew. Chem. Int. Ed. 2013; 52:3993.
30. Slocik JM, Govorov AO, Naik RR. Nano Lett. 2011; 11:701. [PubMed: 21207969]
31. Slocik JM, Stone MO, Naik RR. Small. 2005; 1:1048. [PubMed: 17193392]
32. Fan Z, Govorov AO. J. Phys. Chem. C. 2011; 115:13254.
33. Draine BT, Flatau PJ. J. Opt. Soc. Am. A. 1994; 11:1491.
34. Draine BT, Flatau PJ. 2012 arXiv:1202.3424[physics.comp-ph].
35. Du Q, Faber V, Gunzburger M. SIAM Rev. 1999; 41:637.
36. Hardin DP, Saff EB. Not. Am. Math. Soc. 2004; 51:1186.
37. Renka R. J. Assoc. Comput. Mach. Trans. Math. Software. 1997; 23:416.
38. Saff EB, Kuijlaars AB. J. Math. Intell. 1997; 19:5.
39. Brongersma ML, Hartman JW, Atwater HA. Phys. Rev. B. 2000; 62:16356.
40. Jain PK, Huang WY, El-Sayed MA. Nano Lett. 2007; 7:2080.
41. Pinchuk AO, Schatz GC. Mat. Sci. Eng. B. 2008; 149:251.
42. Zou SL, Schatz GC. Nanotechnology. 2006; 17:2813.
43. Arnold MD, Blaber MG, Ford MJ, Harris N. Opt. Express. 2010; 18:7528. [PubMed: 20389775]
44. Harris N, Arnold MD, Blaber MG, Ford MJ. J. Phys. Chem. C. 2009; 113:2784.
45. Arnold MD, Blaber MG. Opt. Express. 2009; 17:3835. [PubMed: 19259225]

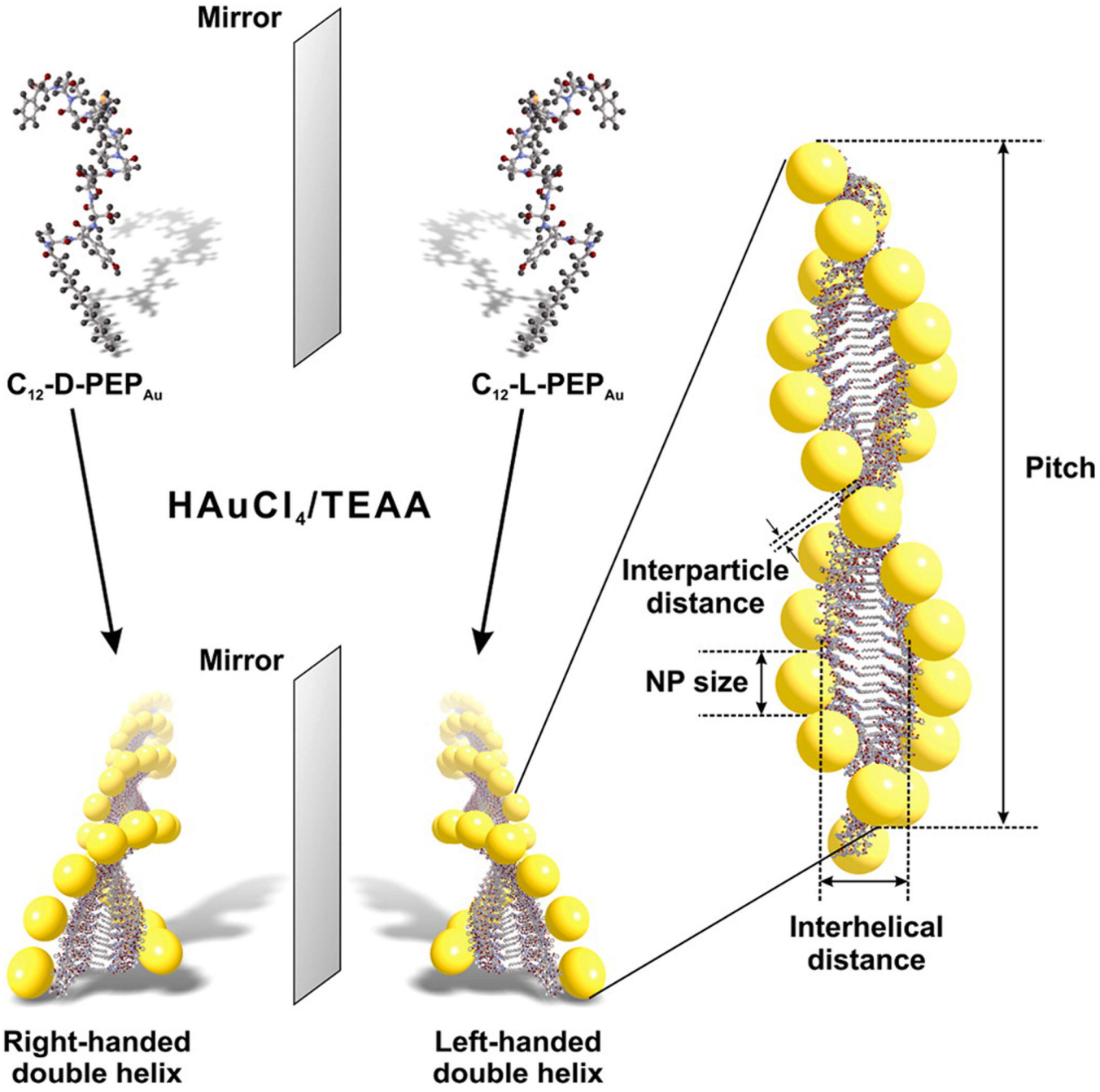

Figure 1.

Scheme detailing the preparation of enantiomeric gold nanoparticle double helices. C_{12}-d-PEP_{Au} and C_{12}-l-PEP_{Au}, when mixed with a gold precursor solution and HEPES buffer, direct the formation of, respectively, right- and left-handed double helices. Each double helix has quantifiable metrics, including nanoparticle size, interparticle distance, pitch, and interhelical distance.

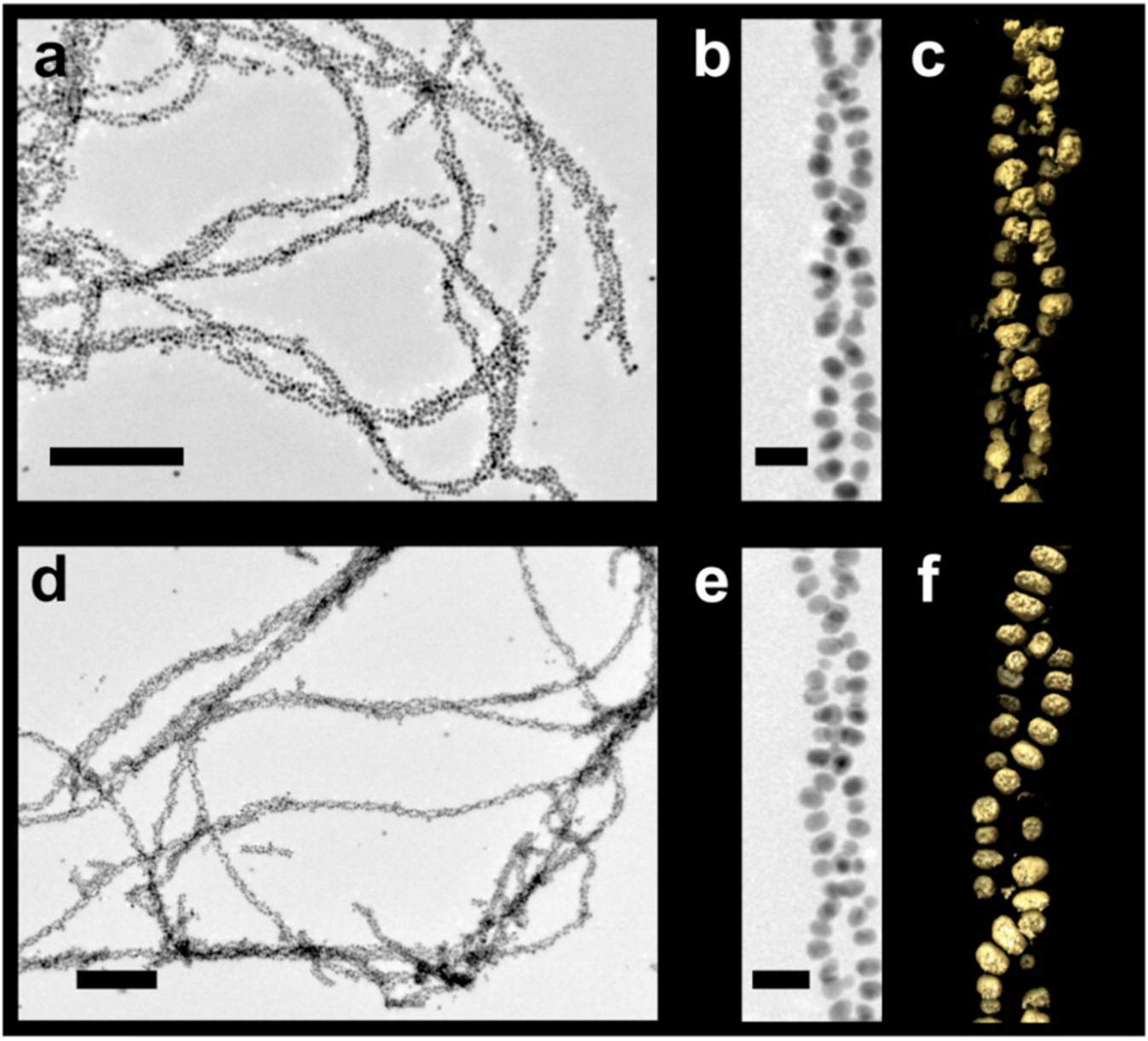

Figure 2.

Transmission electron microscopy (TEM) and electron tomography data. TEM images of left- and right-handed (a,b and d,e, respectively) gold nanoparticle double helices (scale bars: a,d, 200 nm; b,e, 20 nm). The 3D surface renderings of the tomographic volumes reveal the left- or right-handed nature of double helices (c,f, respectively).

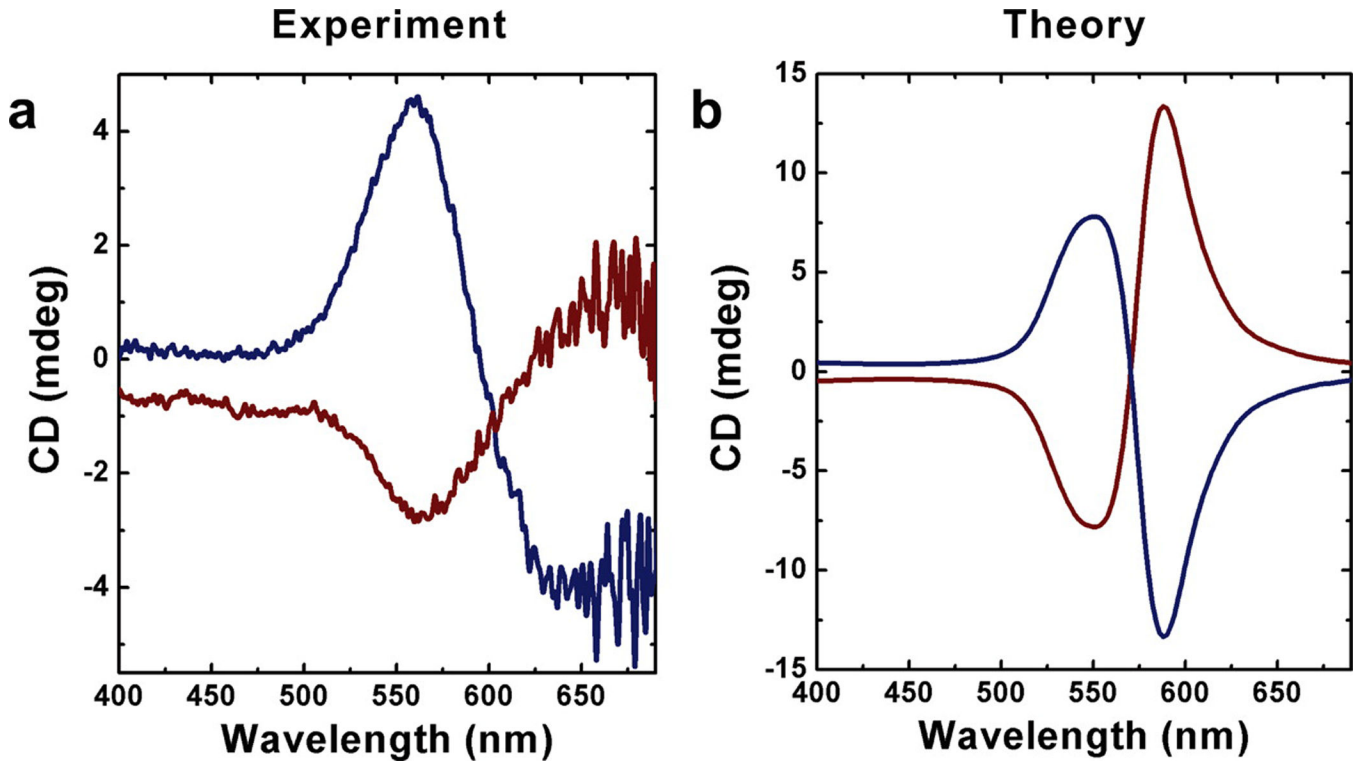

Figure 3.

Experimental and theoretical circular dichroism data for left- and right-handed gold nanoparticle double helices. (a) CD spectra of left-handed (blue) and right-handed (red) gold nanoparticle double helices. Left-handed and right-handed double helices result in vertically mirrored CD signals at 562 nm. (b) CD spectra predicted by the theoretical model exhibit similar bisignate signatures to (a) in the visible region (particle diameter 7 nm). The optical path length is 1 mm.

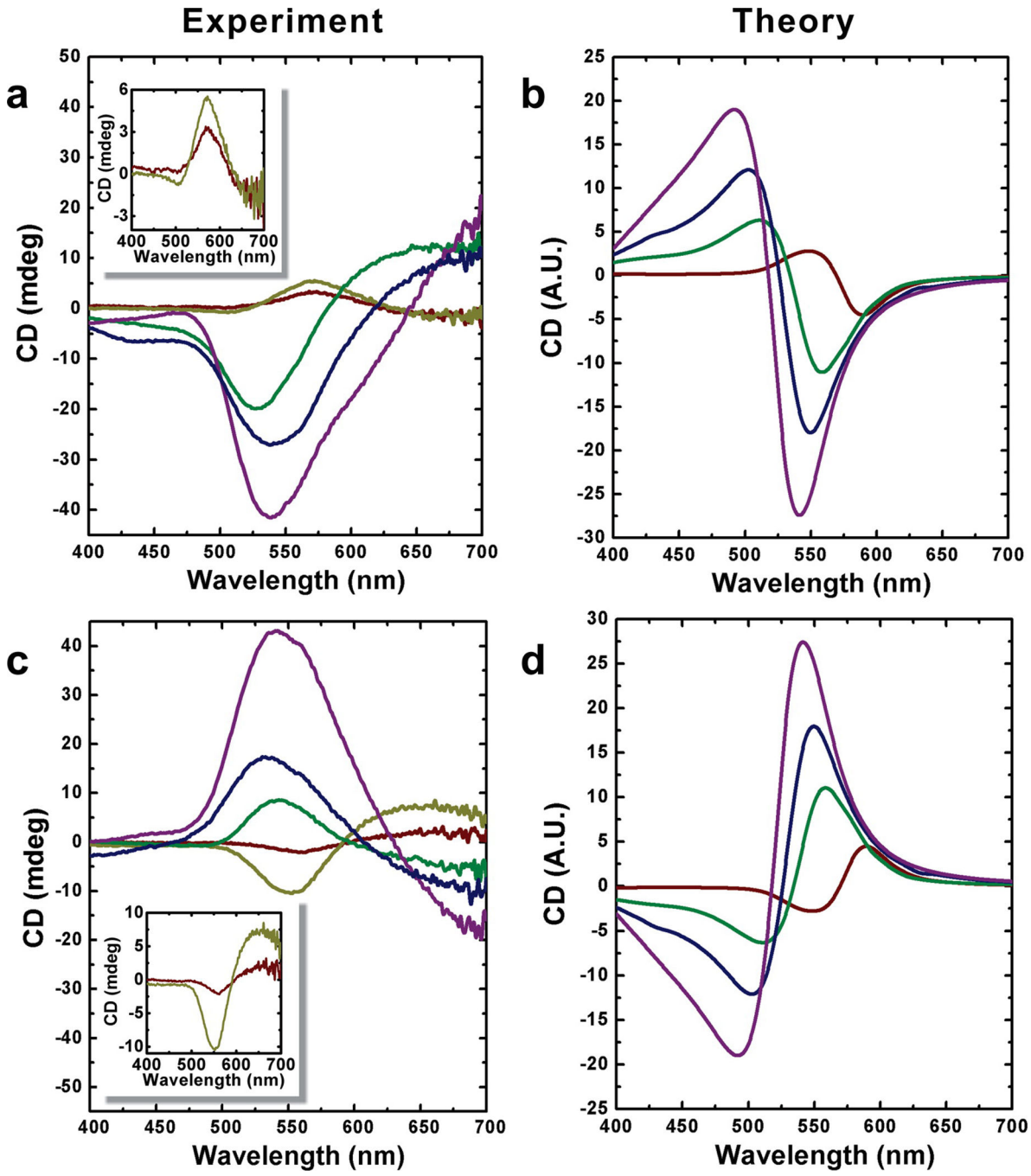

Figure 4.

Experimental and theoretical circular dichroism of gold nanoparticle double helices enhanced by silver. Left- (a) and right-handed (c) gold nanoparticle double helices coated with varied thickness of silver exhibit different CD intensities and wavelengths from the typical gold nanoparticle double helices. A significant blue shift of the peaks (from ~560 to ~530 nm) and dramatically increased amplitudes in the CD spectra were obtained by coating gold nanoparticles with increasing amounts of silver (red, no silver shell; yellow, ~0.5 nm silver shell; green, ~1 nm silver shell; blue, ~2 nm silver shell; purple, ~3 nm silver shell).

The insets in (a) and (c) are provided for clarity. Simulated CD spectra for left- (b) and right-handed (d) gold nanoparticle double helices coated with varied thickness of silver shells (red, no silver shell; green, ~1 nm silver shell; blue, ~1.5 nm silver shell; purple, ~2 nm silver shell).